JACS
JOURNAL OF THE AMERICAN CHEMICAL SOCIETY
pubs.acs.org/JACS
Article

Interaction of Photogenerated Spin Qubit Pairs with a Third Electron Spin in DNA Hairpins

Emmaline R. Lorenzo,[†] Jacob H. Olshansky,[†] Daniel S. D. Abia, Matthew D. Krzyaniak, Ryan M. Young, and Michael R. Wasielewski*

Cite This: J. Am. Chem. Soc. 2021, 143, 4625−4632
Read Online
ACCESS | Metrics & More | Article Recommendations | Supporting Information

ABSTRACT: The designing of tunable molecular systems that can host spin qubits is a promising strategy for advancing the development of quantum information science (QIS) applications. Photogenerated radical pairs are good spin qubit pair (SQP) candidates because they can be initialized in a pure quantum state that exhibits relatively long coherence times. DNA is a well-studied molecular system that allows for control of energetics and spatial specificity through careful design and thus serves as a tunable scaffold on which to control multispin interactions. Here, we examine a series of DNA hairpins that use naphthalenediimide (NDI) as the hairpin linker. Photoexcitation of the NDI leads to subnanosecond oxidation of guanine (G) within the duplex or a stilbenediether (Sd) end-cap to give $NDI^{\bullet-}$-$G^{\bullet+}$ or $NDI^{\bullet-}$-$Sd^{\bullet+}$ SQPs, respectively. A 2,2,6,6-tetramethylpiperdinyl-1-oxyl (TEMPO) stable radical is covalently attached to the hairpin at varying distances from the SQP spins. While TEMPO has a minimal effect on the SQP formation and decay dynamics, EPR spectroscopy indicates that there are significant spin−spin dipolar interactions between the SQP and TEMPO. We also demonstrate the ability to implement more complex spin manipulations of the $NDI^{\bullet-}$-$Sd^{\bullet+}$-TEMPO system using pulse-EPR techniques, which is important for developing DNA hairpins for QIS applications.

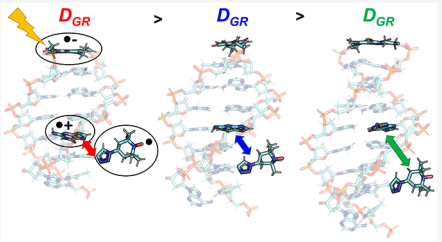

INTRODUCTION

An important goal of quantum information science (QIS) is the search for optimal materials to utilize as quantum bits, or qubits.[1−3] In contrast to classical two-state bits, qubits provide an exponential increase in computational power and speed that is promising for vastly expanding computation and other information technologies.[1,4] The design of qubits requires, in part, that they be initialized in a pure quantum state and have long coherence times.[5] Photogenerated radical pairs are promising candidates for meeting these criteria because photoexcitation of an organic chromophore followed by charge transfer between the chromophore and a neighboring molecule can result in an entangled spin pair that exists in a pure initial singlet quantum state (m_s = 0).[6−12] SQP coherence lifetimes on the order of microseconds have been demonstrated at temperatures as high as 85 K, which in some cases is sufficiently long enough to implement more complex spin manipulations.[13]

The scope of SQP functionality and applicability can be further improved by adding a stable radical to the system as a third spin qubit.[14−19] We have implemented this strategy using a variety of covalent donor−acceptor-radical (D-A-$R^{\bullet}$) triads.[7−10,20] The spin−spin interactions between the $D^{\bullet+}$-$A^{\bullet-}$SQP and $R^{\bullet}$ demonstrate a wide range of phenomena, including control of the SQP lifetime,[7] spin polarization transfer from the SQP to $R^{\bullet}$,[8,10] spin-selective photoreduction of $R^{\bullet}$,[9] and quantum teleportation of the $R^{\bullet}$ electron spin state.[20] The ability to control the spin dynamics of a three-spin system is desirable for achieving certain quantum computing benchmarks by providing a means to implement quantum algorithms.[13,21,22]

While the control and tunability of a three-spin system are clearly favorable for QIS applications, designing and synthesizing a variety of D-A-$R^{\bullet}$ systems that have the correct charge transfer energetics and spin−spin interactions can be difficult. The ability to easily modify the identity of each component of a system allows for more rapid progress in producing an optimal system. The intersection of the more mature field of charge transfer in synthetic DNA structures and the emerging search for molecular qubits now offers the possibility to create an easily modifiable framework that can bear multiple tunable electron spins.[23−26] This goal has precedent in our recent work that explores photogenerated SQPs in synthetic DNA.[24,25,27−31] Additionally, different facets of electron spin behavior have been explored in DNA, such as the effect of a stable radical on DNA structure,[32] DNA as a spin filter,[33] and DNA acting as a classical bit.[34] Such studies have paved the way for more complex spin systems to be developed and implemented in a DNA framework, which will allow for

Received: December 4, 2020
Published: March 18, 2021

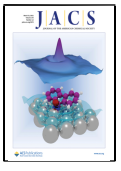

https://doi.org/10.1021/jacs.0c12645
J. Am. Chem. Soc. 2021, 143, 4625−4632

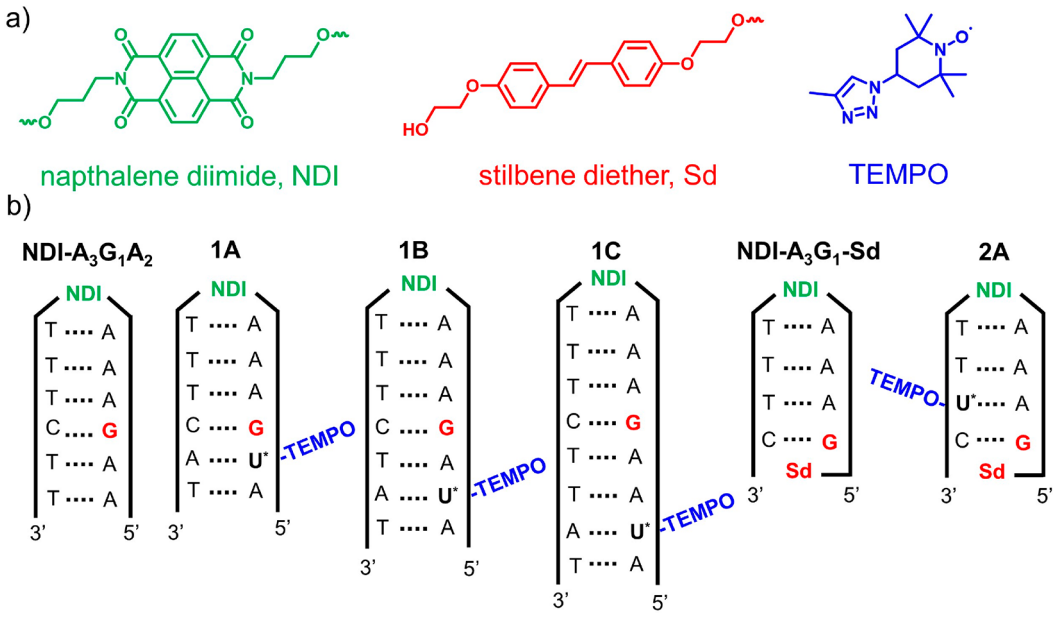

Figure 1. (a) The structures of the chromophore/hole donor NDI (green), the terminal hole acceptor, either guanine or Sd (red), and stable radical, TEMPO (blue). (b) The structure of all DNA hairpins explored in the present work.

exploration of QIS phenomena embedded in a structurally well-defined system.

Charge transport in DNA occurs primarily by hole transport between purine bases.[35] A wide array of DNA hairpins having different chromophoric hairpin linkers, base sequences, and synthetic base pairs have been explored.[29,36−39] Upon photoexcitation of the hairpin linker chromophore, charge transfer occurs via fast hole injection into an adjacent adenine and subsequent hole transfer through an A-tract followed by hole trapping at a guanine or other easy to oxidize molecule covalently linked to the hairpin as a terminal end-cap. Such synthetically modified hairpin structures create long-lived SQPs in large enough quantum yields to be studied with transient optical and EPR spectroscopies.[31,38] A range of chromophores and terminal end-caps have been shown to provide different design advantages, like unique energetics and radical *g*-factors, allowing favorable spectral resolution.[25,29] With the inclusion of an ethynylated uridine nucleobase in the DNA sequence, a stable radical can be covalently attached with relative ease and specificity using click chemistry.[40,41]

In the work presented here, we have designed and synthesized a series of DNA hairpins to explore the interaction of a SQP with a stable radical. A naphthalenediimide (NDI, electron acceptor/hole donor) chromophore is used to covalently link two single DNA strands to form a DNA hairpin. Photoexcitation of NDI generates a SQP comprising $NDI^{\bullet-}$ and a radical cation residing on either guanine or stilbenediether (Sd) covalently bound as the end-cap on the sequence (see structures in Figure 1). The 2,2,6,6-tetramethylpiperdinyl-1-oxyl (TEMPO) radical furnishes the third electron spin and is covalently bound to uridine. The charge transfer and spin dynamics of these hairpins are benchmarked against their counterparts without a stable radical using both transient optical and EPR spectroscopies.

EXPERIMENTAL SECTION

Synthesis. Preparation and characterization of TEMPO derivatives and the DNA hairpins are detailed in the Supporting Information.

Optical Spectroscopy. The femtosecond and nanosecond transient absorption (TA) instrumentation has been described previously.[42] A brief description of the apparatus and details of the sample preparation are given in the Supporting Information (SI).

EPR Spectroscopy. All EPR measurements were performed on 200−300 μM solutions of DNA conjugates in 50% aqueous buffer (100 mM sodium chloride and 10 mM sodium phosphate buffer) and 50% glycerol. The buffer for pulse-EPR experiments used 50% D_2O and 50% glycerol-d_3 (both 95% *d*). Samples were photoexcited at 355 nm (7 ns, 10 Hz) from the frequency-tripled output of a Nd:YAG laser. Experiments were performed at both X-band and Q-band.

X-band measurements. Measurements were made at X-band (~9.6 GHz) on a Bruker Elexsys E680 X/W EPR spectrometer with a split ring resonator (ER4118X-MS3). The temperature was set to 85 K, controlled by an Oxford Instruments CF935 continuous flow optical cryostat with liquid nitrogen. Solutions (~10 μL, ~2 nmol) were loaded into quartz tubes (2.40 mm o.d., 2.00 mm i.d.), subjected to three freeze−pump−thaw cycles on a vacuum line (10^{-4} Torr), and sealed with a hydrogen torch. The samples were prefrozen in liquid nitrogen before inserting into the precooled instrument. Light from the pulsed laser was coupled through an optical fiber placed outside the cryostat window (~2 mJ/pulse), with some portion of the light passing through the coils of the resonator and exciting the sample.

Q-band measurements. Measurements were performed on a laboratory-built Q-band (33.5 GHz) spectrometer described previously.[20] A Bruker Q-band EN 5107D2 resonator was used, and the sample temperature was maintained at 85 K using an Oxford Instruments CF935 Cryostat and an ITC503S temperature controller. Hairpin solutions (~10 μL, ~2 nmol) were loaded into quartz tubes (1.80 mm o.d., 1.50 mm i.d.). The tubes were fitted with a length of optical fiber (Thorlabs, 0.39 numerical aperture, 1 mm diameter, ~1 m length, with ~5−10 cm at the end unprotected by cladding). The optical fiber was fed through a Bruker sample holder and positioned so that the fiber was terminated ~0.5 cm above the top of the sample. The fiber and quartz tube were sealed together using 2 cm of heat-shrink tubing. The samples were prefrozen before inserting into the precooled instrument. The optical fiber was then coupled to a longer optical fiber that received the output from the pulsed laser (0.3 mJ/pulse incident on the sample).

Transient CW EPR. Measurements using continuous wave (CW) microwaves and direct detection were performed at X-band. Following photoexcitation, kinetic traces of transient magnetization under CW microwave irradiation were obtained in both the real and

https://doi.org/10.1021/jacs.0c12645
J. Am. Chem. Soc. 2021, 143, 4625−4632

imaginary channels (quadrature detection). Time traces were recorded over a range of magnetic fields to give 2D spectra. Spectra were processed by first subtracting the signal prior to the laser pulse for each kinetic trace (at a given magnetic field point), and then subtracting the signal average at off-resonance magnetic field points from the spectra obtained at a given time.

Pulse-EPR. Measurements were performed at both X-band and Q-band. Field swept electron echo experiments were performed at X-band and Q-band with a 200 ns delay between the laser flash and the $\pi/2$ pulse. At X-band, the $\pi/2$ and π pulse lengths were 16 and 32 ns, respectively, separated by a time τ = 200 ns. The light and dark signals were collected with separate back-to-back scans, and the difference between the spectra gave the light-dark (L-D) signal. At Q-band the $\pi/2$ and π pulse lengths were 40 and 80 ns, respectively, separated by a time τ = 200 ns. A four-step phase cycle was used, and a "dark" pulse sequence and detection was performed 50 ms after each laser flash (run at 10 Hz). This allowed for the collection of a light and dark signal in a single scan. Signals were detected in quadrature and phased to give absorptive signals (of stable radicals) in the real channel and derivative signals in the imaginary channel. The dark signal, which shows the presence of a stable radical impurity, was subtracted from the light signal to give the photogenerated field swept echo. The echo was integrated at every field point to give echo intensity vs field. Out-of-phase electron spin echo envelope modulation (OOP-ESEEM) experiments were performed at X-band.[43−45] The parameters were the same as the field swept electron echo experiment, except that the time, τ, was increased incrementally between the $\pi/2$ and π pulses.

RESULTS AND DISCUSSION

DNA Hairpin Design. Previous work on the DNA hairpin **NDI-$A_3G_1A_2$** in Figure 1 has shown that photoexcitation of NDI with a 355 nm laser pulse leads to hole injection into the A_3 sequence followed by hole trapping at guanine in 20% yield to produce $NDI^{\bullet-}$-A_3-$G_1^{\bullet+}$-A_2, which has slow charge recombination dynamics.[31,39,46] Series 1 is designed to probe how distance affects the interaction between the spins of the TEMPO radical and $G^{\bullet+}$ in the $NDI^{\bullet-}$-$G^{\bullet+}$ SQP.[31] Series 2 utilizes Sd as the hole acceptor because Sd is much easier to oxidize than G, leading to higher charge separation yields and longer SQP lifetimes, which increase EPR signal intensities and allow for implementation of pulse-EPR techniques.[31] The sequences were synthesized using standard solid-phase oligonucleotide synthetic procedures (see SI).

In order to incorporate TEMPO into the DNA structure, we used a postsynthetic modification strategy. A commercially available synthetic base, 5-ethynyl-2'deoxyuridine (Scheme 1), was incorporated into the structures during the standard oligonucleotide synthesis. The click chemistry reaction scheme shown in Scheme 1 was used to attach TEMPO to the 5-ethynyluracil base.[40] The DNA hairpin was then cleaved from the solid support and subsequently purified by reverse phase C-18 HPLC. The purity of the hairpins was confirmed via MALDI-TOF spectroscopy (Table S1) and steady state UV−vis spectroscopy (Figures S1). In addition, assembly of the duplexes into B-form DNA was confirmed by circular dichroism spectroscopy (Figure S2)

Scheme 1. Click Chemistry Reaction Scheme Utilized to Attach TEMPO to Ethynyluridine, Showing Only the Nucleobase Involved in the Reaction

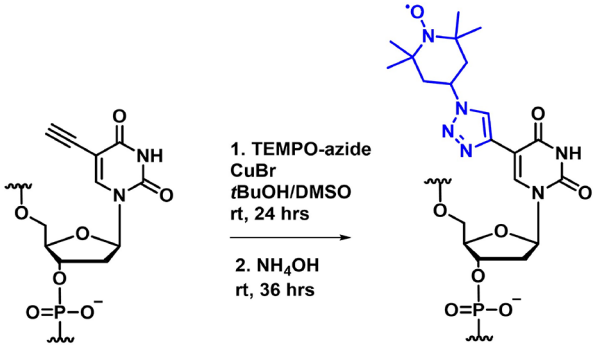

Charge Transfer Dynamics. The charge transfer dynamics following photoexcitation were explored with TA spectroscopy to ascertain how the inclusion of TEMPO affects these dynamics. **NDI-$A_3G_1A_2$** and **NDI-A_3G_1-Sd** were used as the reference hairpins for series 1 and 2, respectively. Following selective photoexcitation of NDI, the TA spectra (Figures 2, S3, and S5) all show absorption features characteristic of $NDI^{\bullet-}$ at 480 and 610 nm, which appear within the ∼300 fs instrument response function.[47] There is no evidence of significant ^{3}*NDI formation from ^{1}*NDI.[48] The features for the A-tract polaron and $G^{\bullet+}$ are too weak to spectrally identify but tracking the time evolution of $NDI^{\bullet-}$ is sufficient to determine the $NDI^{\bullet-}$-$G^{\bullet+}$ lifetimes.[49] For structure **2A**, the characteristic $Sd^{\bullet+}$ radical cation feature at 530 nm was observed in addition to the same spectral NDI features as seen in the control hairpin (Figure S5).[50]

We compare the charge recombination time constants between the hairpins with and without TEMPO to determine if its presence alters the SQP dynamics. The charge recombination lifetimes were determined by fitting the decay of the $NDI^{\bullet-}$ peak with a triexponential function (Table 1). The first time constant, $\tau_1 \cong 3$ ps, is assigned to recombination of the initial contact SQP comprising $NDI^{\bullet-}$ and the neighboring $A^{\bullet+}$. The second time constant (τ_2) is assigned to recombination of the delocalized hole within the A-tract, and the third time constant (τ_3) is attributed to recombination from $G^{\bullet+}$.[31] Comparing these dynamics to the **NDI-$A_3G_1A_2$** control compound for series 1, we observe that charge recombination occurs on similar time scales for these three processes. Approximately the same dynamics are observed for **2A** and **NDI-A_3G_1-Sd** with the addition of a longer component, τ_4, which is assigned to recombination of $NDI^{\bullet-}$-$Sd^{\bullet+}$. The charge recombination time for **NDI-A_3-G_1-Sd** is faster than that of **2A**, which may result from structural distortion of the hairpin caused by the attached TEMPO, as evidenced by the circular dichroism (Figure S2) and EPR data (see below). On the basis of the Marcus-Levich-Jortner model, the charge recombination rate is directly proportional to the square of the electronic coupling matrix element, which is affected by structural distortion.[47] Thus, even a small change in coupling can impact the observed charge recombination rates.

Overall, these results demonstrate that the attachment of TEMPO to the DNA hairpin does not significantly alter the charge transfer dynamics of the series 1 systems and increases all the charge recombination times for **2A** by less than a factor of 2. This suggests that any differences observed in the EPR spectra are due, in large part, to spin dynamics and not differences in the charge transfer/population dynamics.

Spin Dynamics. We next probed the spin dynamics to see the effect of the TEMPO electron spin on the SQP in each structure using several different EPR methods. Continuous wave (CW) EPR spectroscopy without photoexcitation confirmed the presence of TEMPO in all hairpins (Figure S6). Transient continuous wave (TCW) EPR spectroscopy was used to obtain time-resolved spectra of the photogenerated

https://doi.org/10.1021/jacs.0c12645
J. Am. Chem. Soc. 2021, 143, 4625−4632

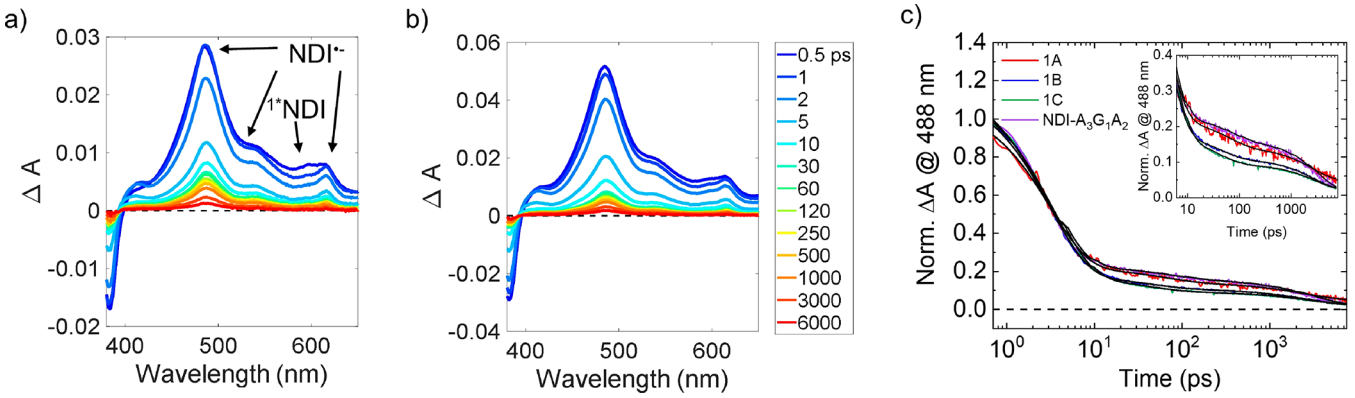

Figure 2. (a) TA spectra of NDI-$A_3G_1A_2$ with the important features of ^{1}*NDI and NDI$^{\bullet-}$ highlighted, (b) TA spectra of hairpin **1B**. (c) Triexponential kinetic fits (black) at 488 nm for **1A**, **1B**, **1C**, and **NDI-$A_3G_1A_2$**.

Table 1. Charge Recombination Time Constants Obtained from Fitting the TA Spectra with a Triexponential Function[a]

Hairpin	τ_1 (ps)	τ_2(ps)	τ_3 (ns)	τ_4 (μs)
1A	3.2	63	2.6	
1B	3.1	44	2.7	
1C	3.3	38	2.6	
NDI-$A_3G_1A_2$	2.8	63	2.8	
2A	2.9	76	17.6	3.4
NDI-A_3G_1-Sd	2.7	67	10.4	2.5

[a]For structures with Sd, a fourth longer lifetime component was obtained. Error bars on kinetic data: $\tau_1 \pm 0.4$ ps, $\tau_2 \pm 10$ ps, $\tau_3 = \pm 0.7$ ns, and $\tau_4 = \pm 0.1$ μs.

SQP. The spectra obtained 100 ns after the laser pulse for each hairpin are shown in Figures 3a-b, with the corresponding simulations overlaid in red. On the basis of the spin-correlated radical pair (SCRP) model,[51,52] a photogenerated SQP produced in an initial singlet state with a positive spin−spin exchange interaction (J) typically exhibits a spin-polarized *e, a, e, a* spectral pattern (*e* = emission, *a* = enhanced absorption, low to high field) arising from two antiphase doublets, each of which is centered at the *g*-value of the individual radical. The spectra of both series 1 and 2 show a somewhat distorted *e, a, e, a* pattern, due to the fact that NDI$^{\bullet-}$ and G$^{\bullet+}$ or Sd$^{\bullet+}$ have similar *g*-factors but significantly different spectral widths, Figure S6. The narrow central features can be assigned to NDI$^{\bullet-}$, while the broader features are assigned to either G$^{\bullet+}$ for series 1 hairpins or Sd$^{\bullet+}$ for series 2 hairpins.[24] The effect of TEMPO on the NDI$^{\bullet-}$-G$^{\bullet+}$ spectra is significant because additional exchange (J_{GR}) and dipolar (D_{GR}) couplings resulting from the TEMPO electron spin can broaden the spectra. However, since J_{GR} depends exponentially on the distance between the spins, J_{GR} should be negligible because of the large number of saturated single bonds between the π system of the neighboring G$^{\bullet+}$ and TEMPO. In contrast, $D_{GR} \propto 1/r^3$, where r is the distance between the spins; thus, as TEMPO is moved closer to G$^{\bullet+}$ in the SQP, D_{GR} increases. This increased coupling results in a larger splitting and thus a broadened spectrum because of the overlap of the NDI$^{\bullet-}$ and G$^{\bullet+}$ resonances, which we observe as a qualitative trend for series 1.

Simulations of **NDI-$A_3G_1A_2$** and **NDI-A_3G_1-Sd** were performed using known or calculated values for the *g*-tensor and hyperfine couplings of NDI$^{\bullet-}$[24] and G$^{\bullet+}$[53] or Sd$^{\bullet+}$[24] and only the relative molecular orientations and the dipolar couplings were varied. The spin−spin coupling was attributed

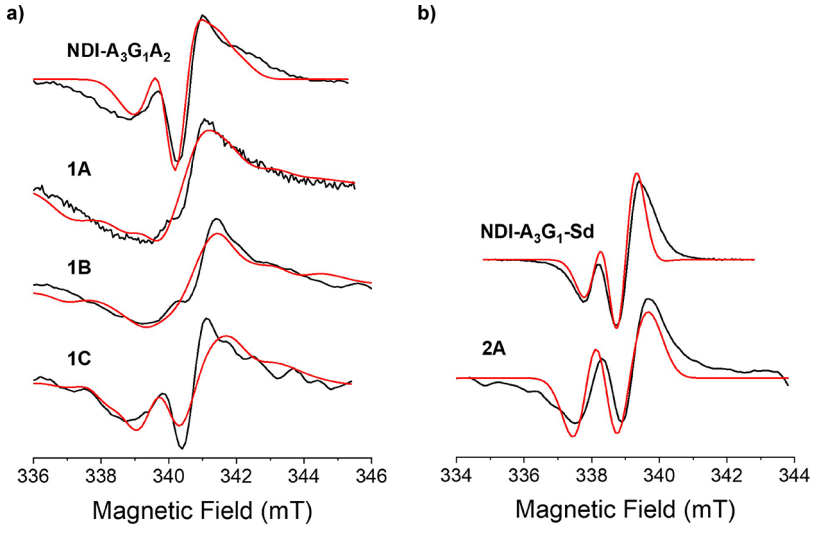

Figure 3. TCW spectra (black traces) at 100 ns following a 355 nm, 7 ns laser pulse for (a) series 1 (b) series 2 overlaid with simulated spectra (red traces).

https://doi.org/10.1021/jacs.0c12645
J. Am. Chem. Soc. 2021, 143, 4625−4632

solely to dipolar coupling, and the exchange coupling was assumed to be negligible and was not considered in the simulations (see SI for details). In order to fit **1A**, **1B**, **1C**, and **2A**, a three-spin model was utilized,[54] where it is assumed that TEMPO has net zero polarization relative to the SQP. The full simulation parameters are provided in Table S2. Due to the fact that the *g*-anisotropy, hyperfine anisotropy, and dipolar coupling are all on the same order of magnitude for measurements performed at 0.34 T (X-band, 9.6 GHz)[55] the simulations are semiquantitative; however, they do provide reasonable estimates for the dipolar coupling, so that assuming the point-dipole approximation,[27] they provide the spin−spin distances and orientations superimposed on the hairpin structures illustrated in Figure 4. It is important to note that the DNA hairpin structure of **2A** is somewhat distorted by the combination of placing the U'-TEMPO base at a position between the NDI hairpin linker and the Sd hole acceptor, which is linked only to the 5′ strand. This results in a longer distance between TEMPO and the $Sd^{\bullet+}$ end-cap.

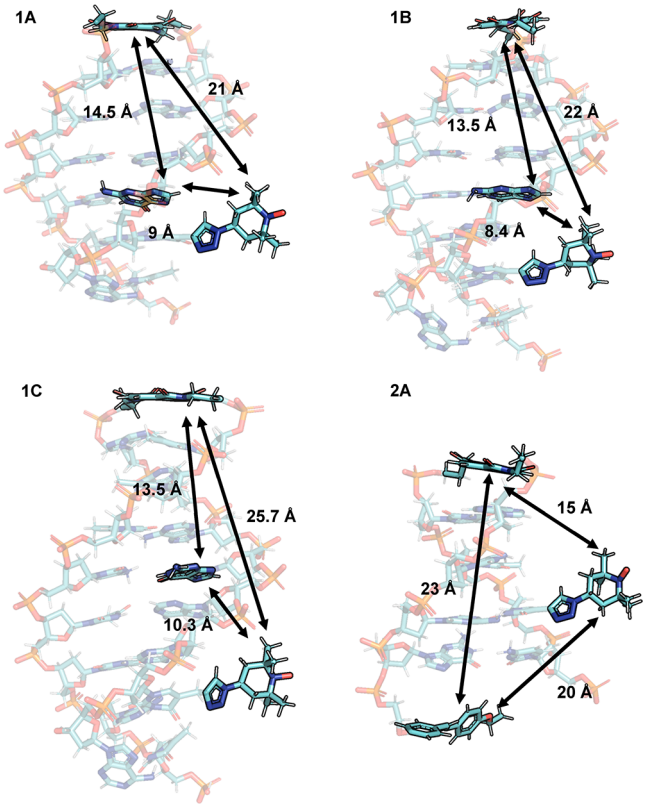

Figure 4. Distances obtained from simulation of the TCW EPR spectra illustrated on the hairpin structures.

In order to perform more complex spin manipulations, a multispin system must be amenable to pulse-EPR experiments. To this end, the photogenerated SQP in hairpin **2A** was subjected to a Hahn two-pulse echo experiment, $\pi/2$-τ−π−τ-echo, where τ is the delay time between the $\pi/2$ and π microwave pulses at both X- and Q-bands (Figure 5a,b, respectively).[56] The field-swept electron spin echo (ESE) spectra were recorded before and after photoexcitation and subtracted to remove the steady-state TEMPO signal. At X-band, *g*-anisotropy, hyperfine anisotropy, and dipolar coupling contribute equally to the observed spectrum, whereas *g*-anisotropy dominates at Q-band. The effect of the *g*-anisotropy of the nitroxide is more apparent at Q-band, so we observe a clearer separation of the nitroxide spectrum from the SQP spectrum, which results in a different spectral appearance of the light minus dark (L-D) subtracted echo signal. The L-D subtracted echo signal allows us to observe only the laser-induced signal, which has little or no contribution from TEMPO, indicating that there is no spin polarization transfer to TEMPO or population depletion of $G^{\bullet+}$ that would result from oxidation of TEMPO by $G^{\bullet+}$. Importantly, the interaction between TEMPO and the spins that constitute the SQP is not sufficiently strong to hyperpolarize TEMPO in these three-spin systems. This result points out the need to design DNA hairpins in which *J* between one of the spins comprising the SQP and the stable third spin is sufficiently large to ensure that the spin entanglement generated by photogeneration of the SQP can be used to implement quantum operations involving the third spin.

When the delay time between the $\pi/2$ and π microwave pulses in the Hahn echo experiment performed on a SQP is scanned, the echo signal from the photogenerated SQP is phase-shifted relative to that of the same spin system at thermal equilibrium and appears with the same phase as the applied microwave pulses.[43] Later theoretical studies showed that this "out-of-phase" (OOP) echo is due to the *J* and *D* spin−spin interactions within the SQP, which modulate the echo decay as a function of τ, so that the overall observed effect is termed out-of-phase electron spin echo envelope modulation (OOP-ESEEM).[44,45]

The OOP-ESEEM signal obtained from the photogenerated SQP in **2A** is an oscillatory signal on top of an exponential

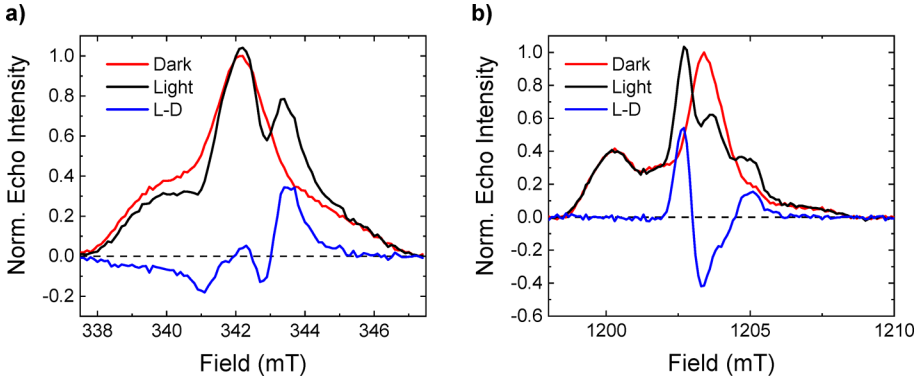

Figure 5. (a) Light (blue), dark (red), and light-minus-dark (L-D, black) electron spin echo signals for hairpin **2A** at X-band and (b) at Q-band.

https://doi.org/10.1021/jacs.0c12645
J. Am. Chem. Soc. 2021, 143, 4625−4632

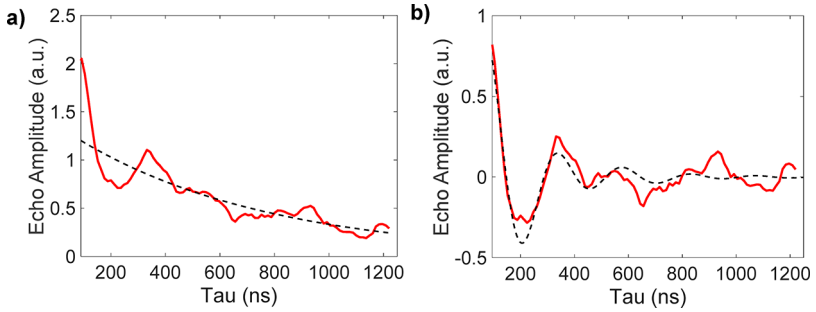

Figure 6. (a) Oscillating echo amplitude signal of **2A** (red) with exponential fit (black) for phase memory time. (b) Echo amplitude signal with exponential fit subtracted (red) and fit (black) used to extract distance of SQP.

decay, and a fit to the exponential yielded a phase memory time T_m = 1.4 μs (Figure 6a), which is on an order of magnitude that can be used to implement quantum gate operations.[13] Subtracting the exponential fit from the data separates the oscillatory component in the data, which was then fit with a function to extract J and D for the SQP (Figure 6b).[57] The fit gives $J \cong 0$ and using the point-dipole approximation,[27] yields a spin−spin distance of 23 Å ± 0.2 Å for the SQP. Our previous work on NDI-Sd hairpins having the same nominal four base pair length gave a spin−spin distance of 18.3 Å.[24] The larger distance in **2A** can be attributed to a structural distortion of the DNA structure by the TEMPO-uridine base that is positioned at a site within the hairpin that is between $NDI^{\bullet-}$ and $G^{\bullet+}$, which is consistent with the difference observed in the charge recombination dynamics for **2A**. This structural distortion from TEMPO could cause the Sd end-cap to rotate away from the hairpin structure since it is only connected on one side, allowing it some degree of flexibility. It is also possible that the TEMPO is distorting the twist of the helix, which could increase the distance between NDI and Sd. However, it should be noted that since the OOP-ESEEM data is fit using a two-spin model, it is also possible that a more sophisticated model is required to accurately represent the effect of the third spin on the OOP-ESEEM of the SQP.

CONCLUSIONS

We successfully synthesized DNA hairpins that have covalently linked TEMPO radicals using postsynthetic click chemistry. Transient optical absorption spectroscopy demonstrates that TEMPO does not have a significant effect on the charge injection or recombination dynamics of the photogenerated $NDI^{\bullet-}$-$G^{\bullet+}$ SQP, and only modestly increases the lifetime of the $NDI^{\bullet-}$-$Sd^{\bullet+}$ SQP, most likely due to structural distortion. In contrast, time-resolved EPR spectroscopy shows that TEMPO has a distance-dependent effect on the SQP, which results from dipolar interaction of the TEMPO electron spin with the SQP. Additionally, field-swept electron spin echo data show that it is possible to spectrally address just the TEMPO spin before photogeneration of the radical pair at X-band. At higher fields such as Q-band or even W-band, TEMPO could be individually addressed before or after photogeneration of the radical pair as a result of increased spectral separation due to g-anisotropy dominating at higher fields. In the future, we will take a similar design approach that uses a stable radical that is more strongly exchange coupled to one spin of the SQP to carry out SQP functions. The tunable architecture of synthetic DNA allows for easy access to structures in which spin−spin interactions among multiple spins can be readily tailored. The fundamental concepts explored in this initial study of a three-spin system in DNA point the way toward new systems that can be employed to implement complex QIS operations, such as spin state teleportation.

ASSOCIATED CONTENT

Supporting Information

The Supporting Information is available free of charge at https://pubs.acs.org/doi/10.1021/jacs.0c12645.

Synthesis and characterization, additional optical and EPR data, and simulation parameters (PDF)

AUTHOR INFORMATION

Corresponding Author

Michael R. Wasielewski − *Department of Chemistry, Center for Molecular Quantum Transduction, and Institute for Sustainability and Energy at Northwestern, Northwestern University, Evanston, Illinois 60208-3113, United States;* orcid.org/0000-0003-2920-5440; Email: m-wasielewski@northwestern.edu

Authors

Emmaline R. Lorenzo − *Department of Chemistry, Center for Molecular Quantum Transduction, and Institute for Sustainability and Energy at Northwestern, Northwestern University, Evanston, Illinois 60208-3113, United States;* orcid.org/0000-0002-0445-3109

Jacob H. Olshansky − *Department of Chemistry, Center for Molecular Quantum Transduction, and Institute for Sustainability and Energy at Northwestern, Northwestern University, Evanston, Illinois 60208-3113, United States;* orcid.org/0000-0003-3658-1487

Daniel S. D. Abia − *Department of Chemistry, Center for Molecular Quantum Transduction, and Institute for Sustainability and Energy at Northwestern, Northwestern University, Evanston, Illinois 60208-3113, United States*

Matthew D. Krzyaniak − *Department of Chemistry, Center for Molecular Quantum Transduction, and Institute for Sustainability and Energy at Northwestern, Northwestern University, Evanston, Illinois 60208-3113, United States;* orcid.org/0000-0002-8761-7323

Ryan M. Young − *Department of Chemistry, Center for Molecular Quantum Transduction, and Institute for Sustainability and Energy at Northwestern, Northwestern University, Evanston, Illinois 60208-3113, United States;* orcid.org/0000-0002-5108-0261

Complete contact information is available at: https://pubs.acs.org/10.1021/jacs.0c12645

Author Contributions

†E.R.L. and J.H.O. contributed equally to this work

Notes

The authors declare no competing financial interest.

■ ACKNOWLEDGMENTS

This work was supported by the National Science Foundation under grant no. CHE-1900422. E.R.L. was supported by a National Science Foundation Graduate Research Fellowship (DGE-1842165).

■ REFERENCES

(1) Harrow, A. W.; Montanaro, A. Quantum computational supremacy. *Nature* **2017**, *549*, 203−209.
(2) Popkin, G. Quest for qubits. *Science* **2016**, *354*, 1090−1093.
(3) Dreyer, C. E.; Alkauskas, A.; Lyons, J. L.; Janotti, A.; Walle, C. G. V. D. First-principles calculations of point defects for quantum technologies. *Annu. Rev. Mater. Res.* **2018**, *48*, 1−26.
(4) Kimble, H. J. The quantum internet. *Nature* **2008**, *453*, 1023−1030.
(5) DiVincenzo, D. P. The physical implementation of quantum computation. *Fortschr. Phys.* **2000**, *48*, 771−783.
(6) Nelson, J. N.; Krzyaniak, M. D.; Horwitz, N. E.; Rugg, B. K.; Phelan, B. T.; Wasielewski, M. R. Zero quantum coherence in a series of covalent spin-correlated radical pairs. *J. Phys. Chem. A* **2017**, *121*, 2241−2252.
(7) Horwitz, N. E.; Phelan, B. T.; Nelson, J. N.; Krzyaniak, M. D.; Wasielewski, M. R. Picosecond control of photogenerated radical pair lifetimes using a stable third radical. *J. Phys. Chem. A* **2016**, *120*, 2841−2853.
(8) Horwitz, N. E.; Phelan, B. T.; Nelson, J. N.; Mauck, C. M.; Krzyaniak, M. D.; Wasielewski, M. R. Spin polarization transfer from a photogenerated radical ion pair to a stable radical controlled by charge recombination. *J. Phys. Chem. A* **2017**, *121*, 4455−4463.
(9) Rugg, B. K.; Phelan, B. T.; Horwitz, N. E.; Young, R. M.; Krzyaniak, M. D.; Ratner, M. A.; Wasielewski, M. R. Spin-selective photoreduction of a stable radical within a covalent donor-acceptor-radical triad. *J. Am. Chem. Soc.* **2017**, *139*, 15660−15663.
(10) Colvin, M. T.; Carmieli, R.; Miura, T.; Richert, S.; Gardner, D. M.; Smeigh, A. L.; Dyar, S. M.; Conron, S. M.; Ratner, M. A.; Wasielewski, M. R. Electron spin polarization transfer from photogenerated spin-correlated radical pairs to a stable radical observer spin. *J. Phys. Chem. A* **2013**, *117*, 5314−5325.
(11) Caregnato, P.; Jarocha, L. E.; Esinhart, H. S.; Lebedeva, N. V.; Tarasov, V. F.; Forbes, M. D. E. Electrostatic control of spin exchange between mobile spin-correlated radical pairs created in micellar solutions. *Langmuir* **2011**, *27*, 5304−5309.
(12) Nelson, J. N.; Zhang, J.; Zhou, J.; Rugg, B. K.; Krzyaniak, M. D.; Wasielewski, M. R. Effect of electron-nuclear hyperfine interactions on multiple-quantum coherences in photogenerated covalent radical (qubit) pairs. *J. Phys. Chem. A* **2018**, *122*, 9392−9402.
(13) Nelson, J. N.; Zhang, J.; Zhou, J.; Rugg, B. K.; Krzyaniak, M. D.; Wasielewski, M. R. CNOT gate operation on a photogenerated molecular electron spin-qubit pair. *J. Chem. Phys.* **2020**, *152*, 014503.
(14) Salikhov, K. M.; Golbeck, J. H.; Stehlik, D. Quantum teleportation across a biological membrane by means of correlated spin pair dynamics in photosynthetic reaction centers. *Appl. Magn. Reson.* **2007**, *31*, 237−252.
(15) Salikhov, K. M.; Van der Est, A. J.; Stehlik, D. The transient EPR spectra and spin dynamics of coupled three-spin systems in photosynthetic reaction centres. *Appl. Magn. Reson.* **2009**, *16*, 101−134.
(16) Kandrashkin, Y. E.; Salikhov, K. M. Numerical simulation of quantum teleportation across biological membrane in photosynthetic reaction centers. *Appl. Magn. Reson.* **2010**, *37*, 549−566.
(17) Volkov, M. Y.; Salikhov, K. M. Pulse protocols for quantum computing with electron spins as qubits. *Appl. Magn. Reson.* **2011**, *41*, 145−154.
(18) Borovkov, V. I.; Ivanishko, I. S.; Bagryansky, V. A.; Molin, Y. N. Spin-selective reaction with a third radical destroys spin correlation in the surviving radical pairs. *J. Phys. Chem. A* **2013**, *117*, 1692−1696.
(19) Bagryansky, V. A.; Borovkov, V. I.; Bessmertnykh, A. O.; Tretyakova, I. S.; Beregovaya, I. V.; Molin, Y. N. Interaction of spin-correlated radical pair with a third radical: Combined effect of spin-exchange interaction and spin-selective reaction. *J. Chem. Phys.* **2019**, *151*, 224308.
(20) Rugg, B. K.; Krzyaniak, M. D.; Phelan, B. T.; Ratner, M. A.; Young, R. M.; Wasielewski, M. R. Photodriven quantum teleportation of an electron spin state in a covalent donor-acceptor-radical system. *Nat. Chem.* **2019**, *11*, 981−986.
(21) Cao, C.; Han, Y.-H.; Zhang, L.; Fan, L.; Duan, Y.-W.; Zhang, R. High-fidelity universal quantum controlled gates on electron-spin qubits in quantum dots inside single-sided optical microcavities. *Advanced Quantum Technologies* **2019**, *2*, 1900081.
(22) Sun, Y.; Xu, P.; Chen, P.-X.; Liu, L. Controlled phase gate protocol for neutral atoms via off-resonant modulated driving. *Phys. Rev. Appl.* **2020**, *13*, 024059.
(23) Yamamoto, S.; Nakazawa, S.; Sugisaki, K.; Maekawa, K.; Sato, K.; Toyota, K.; Shiomi, D.; Takui, T. Structural determination of a DNA oligomer for a molecular spin qubit Lloyd model of quantum computers. *Z. Phys. Chem. (N. F.)* **2017**, *231*, 439−458.
(24) Olshansky, J. H.; Krzyaniak, M. D.; Young, R. M.; Wasielewski, M. R. Photogenerated spin-entangled qubit (radical) pairs in DNA hairpins: Observation of spin delocalization and coherence. *J. Am. Chem. Soc.* **2019**, *141*, 2152−2160.
(25) Olshansky, J. H.; Zhang, J.; Krzyaniak, M. D.; Lorenzo, E. R.; Wasielewski, M. R. Selectively addressable photogenerated spin qubit pairs in DNA hairpins. *J. Am. Chem. Soc.* **2020**, *142*, 3346−3350.
(26) Nakajima, S.; Akiyama, K.; Kawai, K.; Takada, T.; Ikoma, T.; Majima, T.; Tero-Kubota, S. Spin-correlated radical pairs in synthetic hairpin DNA. *ChemPhysChem* **2007**, *8*, 507−509.
(27) Carmieli, R.; Smeigh, A. L.; Mickley Conron, S. M.; Thazhathveetil, A. K.; Fuki, M.; Kobori, Y.; Lewis, F. D.; Wasielewski, M. R. Structure and dynamics of photogenerated triplet radical ion pairs in DNA hairpin conjugates with anthraquinone end caps. *J. Am. Chem. Soc.* **2012**, *134*, 11251−11260.
(28) Carmieli, R.; Thazhathveetil, A. K.; Lewis, F. D.; Wasielewski, M. R. Photoselective DNA hairpin spin switches. *J. Am. Chem. Soc.* **2013**, *135*, 10970−10973.
(29) Carmieli, R.; Zeidan, T. A.; Kelley, R. F.; Mi, Q.; Lewis, F. D.; Wasielewski, M. R. Excited state, charge transfer, and spin dynamics in DNA hairpin conjugates with perylenediimide hairpin linkers. *J. Phys. Chem. A* **2009**, *113*, 4691−4700.
(30) Zeidan, T. A.; Carmieli, R.; Kelley, R. F.; Wilson, T. M.; Lewis, F. D.; Wasielewski, M. R. Charge-transfer and spin dynamics in DNA hairpin conjugates with perylenediimide as a base-pair surrogate. *J. Am. Chem. Soc.* **2008**, *130*, 13945−13955.
(31) Olshansky, J. H.; Young, R. M.; Wasielewski, M. R. Charge separation and recombination pathways in diblock DNA hairpins. *J. Phys. Chem. B* **2019**, *123*, 1545−1553.
(32) Gophane, D. B.; Sigurdsson, S. T. Tempo-derived spin labels linked to the nucleobases adenine and cytosine for probing local structural perturbations in DNA by EPR spectroscopy. *Beilstein J. Org. Chem.* **2015**, *11*, 219−227.
(33) Göhler, B.; Hamelbeck, V.; Markus, T. Z.; Kettner, M.; Hanne, G. F.; Vager, Z.; Naaman, R.; Zacharias, H. Spin selectivity in electron transmission through self-assembled monolayers of double-stranded DNA. *Science* **2011**, *331*, 894−897.
(34) Sennels, L.; Bentin, T. To DNA, all information is equal. *Artif. DNA PNA XNA* **2012**, *3*, 109−111.
(35) Genereux, J. C.; Barton, J. K. Mechanisms for DNA charge transport. *Chem. Rev.* **2010**, *110*, 1642−1662.
(36) Brown, K. E.; Singh, A. P. N.; Wu, Y. L.; Mishra, A. K.; Zhou, J.; Lewis, F. D.; Young, R. M.; Wasielewski, M. R. Tracking hole

https://doi.org/10.1021/jacs.0c12645
J. Am. Chem. Soc. 2021, 143, 4625−4632

transport in DNA hairpins using a phenylethynylguanine nucleobase. *J. Am. Chem. Soc.* **2017**, *139*, 12084−12092.
(37) Lewis, F. D.; Letsinger, R. L.; Wasielewski, M. R. Dynamics of photoinduced charge transfer and hole transport in synthetic DNA hairpins. *Acc. Chem. Res.* **2001**, *34*, 159−170.
(38) Lewis, F. D.; Young, R. M.; Wasielewski, M. R. Tracking photoinduced charge separation in DNA: From start to finish. *Acc. Chem. Res.* **2018**, *51*, 1746−1754.
(39) Singh, A. P.; Harris, M. A.; Young, R. M.; Miller, S. A.; Wasielewski, M. R.; Lewis, F. D. Raising the barrier for photoinduced DNA charge injection with a cyclohexyl artificial base pair. *Faraday Discuss.* **2015**, *185*, 105−120.
(40) Jakobsen, U.; Shelke, S. A.; Vogel, S.; Sigurdsson, S. T. Site-directed spin-labeling of nucleic acids by click chemistry: Detection of abasic sites in duplex DNA by EPR spectroscopy. *J. Am. Chem. Soc.* **2010**, *132*, 10424−10428.
(41) Snorri Th, S. Nitroxides and nucleic acids: Chemistry and electron paramagnetic resonance (EPR) spectroscopy. *Pure Appl. Chem.* **2011**, *83*, 677−686.
(42) Young, R. M.; Dyar, S. M.; Barnes, J. C.; Juríček, M.; Stoddart, J. F.; Co, D. T.; Wasielewski, M. R. Ultrafast conformational dynamics of electron transfer in exbox^{4+}⊂perylene. *J. Phys. Chem. A* **2013**, *117*, 12438−12448.
(43) Thurnauer, M. C.; Norris, J. R. An electron spin echo phase shift observed in photosynthetic algae: Possible evidence for dynamic radical pair interactions. *Chem. Phys. Lett.* **1980**, *76*, 557−561.
(44) Salikhov, K. M.; Kandrashkin, Y. E.; Salikhov, A. K. Peculiarities of free induction and primary spin echo signals for spin-correlated radical pairs. *Appl. Magn. Reson.* **1992**, *3*, 199−216.
(45) Tang, J.; Thurnauer, M. C.; Norris, J. R. Electron spin echo envelope modulation due to exchange and dipolar interactions in a spin-correlated radical pair. *Chem. Phys. Lett.* **1994**, *219*, 283−290.
(46) Renaud, N.; Harris, M. A.; Singh, A. P.; Berlin, Y. A.; Ratner, M. A.; Wasielewski, M. R.; Lewis, F. D.; Grozema, F. C. Deep-hole transfer leads to ultrafast charge migration in DNA hairpins. *Nat. Chem.* **2016**, *8*, 1015−1021.
(47) Lewis, F. D.; Kalgutkar, R. S.; Wu, Y.; Liu, X.; Liu, J.; Hayes, R. T.; Miller, S. E.; Wasielewski, M. R. Driving force dependence of electron transfer dynamics in synthetic DNA hairpins. *J. Am. Chem. Soc.* **2000**, *122*, 12346−12351.
(48) Ganesan, P.; Baggerman, J.; Zhang, H.; Sudholter, E. J. R.; Zuilhof, H. Femtosecond time-resolved photophysics of 1,4,5,8-naphthalene diimides. *J. Phys. Chem. A* **2007**, *111*, 6151−6156.
(49) Harris, M. A.; Mishra, A. K.; Young, R. M.; Brown, K. E.; Wasielewski, M. R.; Lewis, F. D. Direct observation of the hole carriers in DNA photoinduced charge transport. *J. Am. Chem. Soc.* **2016**, *138*, 5491−5494.
(50) Lewis, F. D.; Liu, X.; Wu, Y.; Miller, S. E.; Wasielewski, M. R.; Letsinger, R. L.; Sanishvili, R.; Joachimiak, A.; Tereshko, V.; Egli, M. Structure and photoinduced electron transfer in exceptionally stable synthetic DNA hairpins with stilbenediether linkers. *J. Am. Chem. Soc.* **1999**, *121*, 9905−9906.
(51) Hore, P. J.; Hunter, D. A.; McKie, C. D.; Hoff, A. J. Electron paramagnetic resonance of spin-correlated radical pairs in photosynthetic reactions. *Chem. Phys. Lett.* **1987**, *137*, 495−500.
(52) Closs, G. L.; Forbes, M. D. E.; Norris, J. R. Spin-polarized electron paramagnetic resonance spectra of radical pairs in micelles: Observation of electron spin-spin interactions. *J. Phys. Chem.* **1987**, *91*, 3592−3599.
(53) Adhikary, A.; Kumar, A.; Becker, D.; Sevilla, M. D. The guanine cation radical: Investigation of deprotonation states by ESR and DFT. *J. Phys. Chem. B* **2006**, *110*, 24171−24180.
(54) Salikhov, K. M.; van der Est, A. J.; Stehlik, D. The transient EPR spectra and spin dynamics of coupled three-spin systems in photosynthetic reaction centres. *Appl. Magn. Reson.* **1999**, *16*, 101−134.
(55) Zarea, M.; Carmieli, R.; Ratner, M. A.; Wasielewski, M. R. Spin dynamics of radical pairs with restricted geometries and strong exchange coupling: The role of hyperfine coupling. *J. Phys. Chem. A* **2014**, *118*, 4249−4255.
(56) Hahn, E. L. Spin echoes. *Phys. Rev.* **1950**, *80*, 580−594.
(57) Santabarbara, S.; Kuprov, I.; Hore, P. J.; Casal, A.; Heathcote, P.; Evans, M. C. W. Analysis of the spin-polarized electron spin echo of the $[P700^{+}A_1^{-}]$ radical pair of photosystem I indicates that both reaction center subunits are competent in electron transfer in cyanobacteria, green algae, and higher plants. *Biochemistry* **2006**, *45*, 7389−7403.

https://doi.org/10.1021/jacs.0c12645
J. Am. Chem. Soc. 2021, 143, 4625−4632